

New analysis of the ν_5 and $2\nu_9$ bands of HNO_3 by infrared and millimeter wave techniques: line positions and intensities^{☆,☆☆}

A. Perrin,^{a,*} J. Orphal,^a J.-M. Flaud,^a S. Klee,^b G. Mellau,^b H. Mäder,^c D. Walbrodt,^c and M. Winnewisser^d

^a *Laboratoire de Photophysique Moléculaire, CNRS Université Paris Sud, Bat 350, Campus d'Orsay F-91405, Orsay, Cedex, France*

^b *Physikalisch-Chemisches Institut, Justus-Liebig-Universität, Heinrich-Buff-Ring 58, D-35392, Giessen, Germany*

^c *Institut für Physikalische Chemie, Universität Kiel, Olshausenstrasse 40, D-24098 Kiel, Germany*

^d *Department of Physics, The Ohio State University, Columbus, OH 43210, USA*

Received 21 October 2003; in revised form 20 January 2004

Available online 12 March 2004

Abstract

Nitric acid (HNO_3) plays an important role in the Earth's atmosphere as a reservoir molecule of NO_x species. It has a strong infrared signature at $11\ \mu\text{m}$ which is one of the most commonly used for the infrared retrieval of this species in the atmosphere since this spectral region coincides with an atmospheric window. It is therefore essential to have high quality spectral parameters in this spectral region. The main goal of this work is then to generate as reliable as possible line positions and intensities for the ν_5 and $2\nu_9$ cold bands centered at 879.1075 and $896.4467\ \text{cm}^{-1}$, respectively. In particular the existing line parameters need improvement in the wings of the $11\ \mu\text{m}$ window in order to retrieve more accurately the CFC-11 (CCl_3F) and CFC-12 (CCl_2F_2) atmospheric species at ~ 850 and $\sim 920\ \text{cm}^{-1}$, respectively. This work is also motivated by theoretical considerations. Very strong resonances couple indeed the 5^1 and 9^2 rotational levels. In addition the ν_9 mode (OH torsion) is a "large amplitude" motion, and torsional splittings affect both the $\nu_9 = 2$ and the $\nu_5 = 1$ rotational transitions. In the present study, these effects are accounted for simultaneously both for the line position and line intensity calculations. To calculate the line positions the Hamiltonian matrix accounts for the very strong Fermi and the weaker Coriolis interactions linking the $5^1 \rightleftharpoons 9^2$ rotational levels, and the torsional effects are accounted for within the frame of the IAM (Internal Axis Method) approach. In addition, the v -diagonal blocks involve non-orthorhombic operators together with Watson's type rotational operators. This means that the z -quantization axis deviates from the a inertial axis for both the 5^1 and 9^2 vibrational states. The line intensity calculations were performed accounting also for the axis switching effects. As far as the experimental line positions are concerned we have used the millimeter wave data available in the literature [J. Mol. Spectrosc., 175 (1996) 395; J. Mol. Spectrosc., 208 (2001) 121; and references therein], as well as new centimeter wave measurements performed in Kiel and new Fourier transform infrared spectra recorded in Giessen. For the line intensities we have used an extensive set of individual line intensities measured recently [J. Mol. Spectrosc., 218 (2003) 151]. All these experimental data were very satisfactorily reproduced using the theoretical model described above and an improved set of line positions and intensities was generated for the ν_5 and $2\nu_9$ bands allowing one to better model the HNO_3 absorption in the $11\ \mu\text{m}$ spectral domain.

© 2004 Elsevier Inc. All rights reserved.

1. Introduction

Nitric acid (HNO_3) plays an important role as a "reservoir" molecule for both the NO_x (nitrogen oxides)

and HO_x (hydrogen oxides) species in the stratosphere [1]. These radicals are potentially active contributors to the ozone destruction in the stratosphere through catalytic reactions. For this reason, HNO_3 has been the subject of numerous spectroscopic studies. The $11\ \mu\text{m}$ band which exhibits a strong signature in a rather clear atmospheric window is commonly used for the remote sensing of this species both from satellites or balloons [2–4] or from the ground [5]. This spectral region involves mainly the ν_5 and $2\nu_9$ cold bands located at

[☆] Supplementary data associated with this article can be found in the online version, at [doi:10.1016/j.jms.2004.02.002](https://doi.org/10.1016/j.jms.2004.02.002).

^{☆☆} Paper in the honour of Dr. Jon T. Hougen for his many contributions to science (J. Mol. Spectrosc.).

* Corresponding author. Fax: +33(0)169157530.

E-mail address: agnes.perrin@ppm.u-psud.fr (A. Perrin).

879.1076 and 896.4468 cm^{-1} , respectively, together with two hot bands, namely $\nu_5 + \nu_9 - \nu_9$ which possesses a rather sharp signature at 885.425 cm^{-1} [6] and the much weaker $3\nu_9 - \nu_9$ band at 830.6 cm^{-1} [7,8].

Because of its atmospheric interest, numerous low resolution grating [9–11], high resolution infrared diode laser [12–15], high resolution Fourier transform [6,7,16–19], and microwave [20–22] studies were devoted to the improvement of the line positions or line intensities parameters for the HNO_3 bands at 11 μm .

Recent updates of the spectral 11 μm line parameters were performed in the last versions of the atmospheric databases [23–25]. They concern the line positions and intensities for the two interacting cold bands ν_5 and $2\nu_9$ and the $\nu_5 + \nu_9 - \nu_9$ hot band. However, critical studies of the HNO_3 spectral parameters at 11 μm [6,24,26–29], have shown that improvements are still needed. For example the $\nu_5 + \nu_9 - \nu_9$ hot band at 885.425 cm^{-1} was the subject of a recent infrared study [6].

The goal of the present work is dual: (i) to improve the quality of the line positions and line intensities for the ν_5 and $2\nu_9$ cold bands for atmospheric application, since various problems (absolute intensities, wings of the 11 μm band) were pointed out in recent papers and (ii) to better understand theoretically the spectroscopic properties (resonance, torsion) of this molecule.

2. Previous studies for the ν_5 and $2\nu_9$ bands

As already pointed out the 11 μm absorption region of HNO_3 has been the subject of a number of studies and we give in this section an overview of them since numerous previous results are used in this paper.

2.1. Line positions

The first detailed assignments and calculations for the ν_5 and $2\nu_9$ bands of HNO_3 were performed by Maki and Wells [13,15] using diode laser spectra. In [15] only the strong Fermi resonance was accounted for allowing one to calculate the rather limited set of 5^1 and 9^2 energy levels available at that time. Subsequently a more detailed analysis of these two bands was performed using Fourier transform spectra [16,17], and the calculations of line positions and line intensities had to account for both the Fermi and Coriolis resonances. Later on, this infrared analysis was completed by a new calculation [30] using an internal axis method (IAM) formalism and modeling the torsional splittings observed for a few $\nu_5 = 1$ and $\nu_9 = 2$ mm/submm transitions. Three recent papers [20–22] deal with the measurements and the analysis of a much larger set of ν_5 and $2\nu_9$ mm/submm transitions. The first two papers [20,21] deal mainly with transitions not split by asymmetry since they involve low K_a values. In this case, it was sufficient to consider the

Fermi resonance and the torsional splittings were accounted for by using a simplified model (two torsional bands centers for $2\nu_9$). The third paper [22] considers a more extended set of mm/submm measurements, and two calculations “artificial splitting” and “induced splitting” (see Table 4 of [22]) were performed which account both for the Fermi and Coriolis resonances together with the torsional effects which were handled using the internal axis system (IAS) approach. In the “induced splitting” calculation [22,31, 32] the torsional splittings of the ν_5 rotational transitions are assumed to have their physical origin in the very strong vibration–rotation resonances linking the 5^1 and 9^2 energy levels, and a large value ($F_0 = 8.531408(2) \text{cm}^{-1}$) was derived for the zero-order Fermi parameter. In the “artificial splitting” [22] the calculations were performed by setting F_0 to zero and considering that the torsional effects in 5^1 and 9^2 are more or less independent.

2.2. Line intensities and quality of the parameters in the atmospheric databases

In the case of the HNO_3 molecule, the data currently available in the databases [23,25] were derived from the analysis of infrared spectra performed in [16,17] but they are not reliable for extrapolation to the far wings of the band (see Figs. 1 and 2), preventing in particular accurate retrievals of the atmospheric profiles of the CFC-11 (CCl_3F) and CFC-12 (CCl_2F_2) which absorb around 850 and 925 cm^{-1} [33].

When dealing with line intensities for atmospheric retrievals, one faces two problems. The first one concerns the relative intensities which should be consistent in the whole spectral domain. The other problem concerns reliable “absolute” line intensities. This question is still controversial for HNO_3 , since several previous and on-going efforts in various laboratories give results which do not agree. The first studies concerned measurements of the integrated band intensities at 11 μm using low resolution spectra [9–11]. They led to integrated strengths at 300 K varying from 483 to 630 $\text{cm}^{-2} \text{atm}^{-1}$. The situation was not better for line intensity measurements since the results obtained using a diode laser technique [12] and using Fourier transform spectra [17] do not agree: the intensities measured in [17] are on the average about 20% stronger than those of [12]. Also there exists a discrepancy between the low and high resolution measurements. Indeed using a model taking into account the various resonances and fitting the experimental intensities a synthetic spectrum of ν_5 and $2\nu_9$ was generated [17]. Using this calculated spectrum and accounting for the hot band contributions led to an integrated band strength at 11 μm about 30% weaker than the value measured by Giver et al. [10]. All this shows the difficulty of the problem since rather large discrepancies exist between the various results. Finally it is worth stressing that

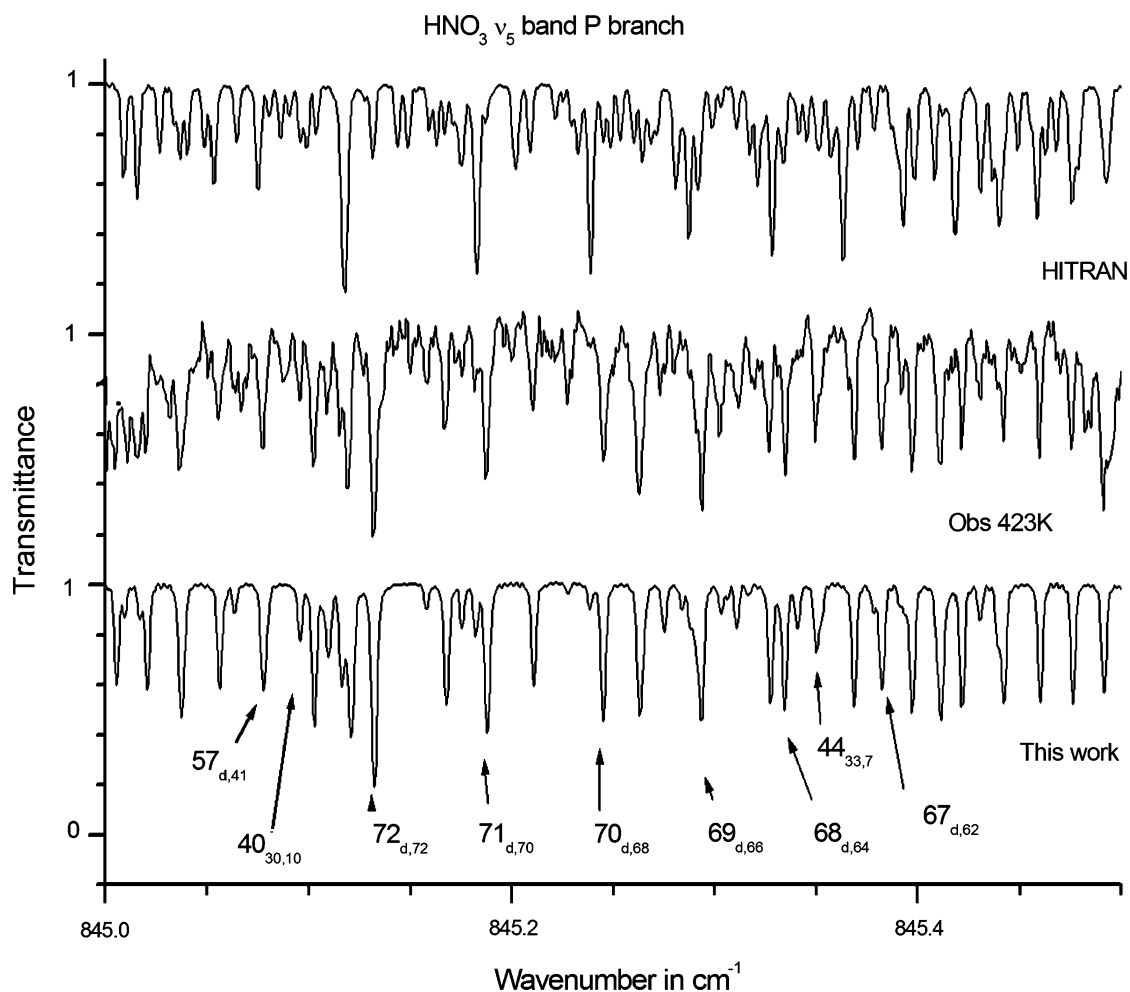


Fig. 1. Part of the P branch of the ν_5 band around 845 cm^{-1} . Upper trace, line by line calculation using the HITRAN line list. Medium trace, observed spectrum recorded at 423 K. Lower trace, line by line calculation (this work). It is obvious that the new calculation is in much better agreement with the observation. Some high J_{K_a, K_c}^{\prime} assignments in the upper state are given (d stands for degenerate transitions with $K_a = J - K_c$ and $K_a = J - K_c + 1$).

the recommendation adopted for the preparation of the HITRAN-96 database [23,24] was to normalize the ν_5 and $2\nu_9$ line list generated in [16,17] to the Giver $11\text{ }\mu\text{m}$ band intensity after a proper hot band correction.

Very recently two new studies were devoted to the measurements of HNO_3 line intensities at $11\text{ }\mu\text{m}$:

- (i) An extensive set of HNO_3 line intensities (733 and 402 for the ν_5 and $2\nu_9$ bands, respectively) were measured using Fourier transform spectra recorded at Kitt Peak [18]. The goal was one more time to measure accurate absolute intensities in the $11\text{ }\mu\text{m}$ region while adopting special experimental precautions to minimize and/or estimate correctly the HNO_3 decomposition [18]. This new list of line intensities is rather complete providing one with a much more extended set of measured intensities and a larger range of rotational quantum numbers than previously observed [17]. On the average these new line intensities are weaker than those in the HITRAN line list: $\text{INT}_{\text{HITRAN}}/\text{INT}_{\text{NEW}} = 1.14 \pm 0.06$.

- (ii) Fourier transform absorbances were measured at PNNL [19] for different samples of nitrogen–nitric acid mixtures at a spectral resolution of 0.112 cm^{-1} and used to determine in particular integrated cross sections for the $11\text{ }\mu\text{m}$ region. For this spectral region, the integrated intensity is about 6% lower than the value reported by Giver [10].

3. Theoretical considerations

The second goal of this study was to test the quality and the applicability of the theoretical model used to reproduce the energy levels and the line intensities of the HNO_3 molecule. For this molecule indeed, two difficult problems have to be handled: the large amplitude torsional splittings which affect *both* the $\nu_9 = 2$ and $\nu_5 = 1$ microwave transitions on the one hand and the very strong resonances which link the 5^1 and 9^2 energy levels on the other hand.

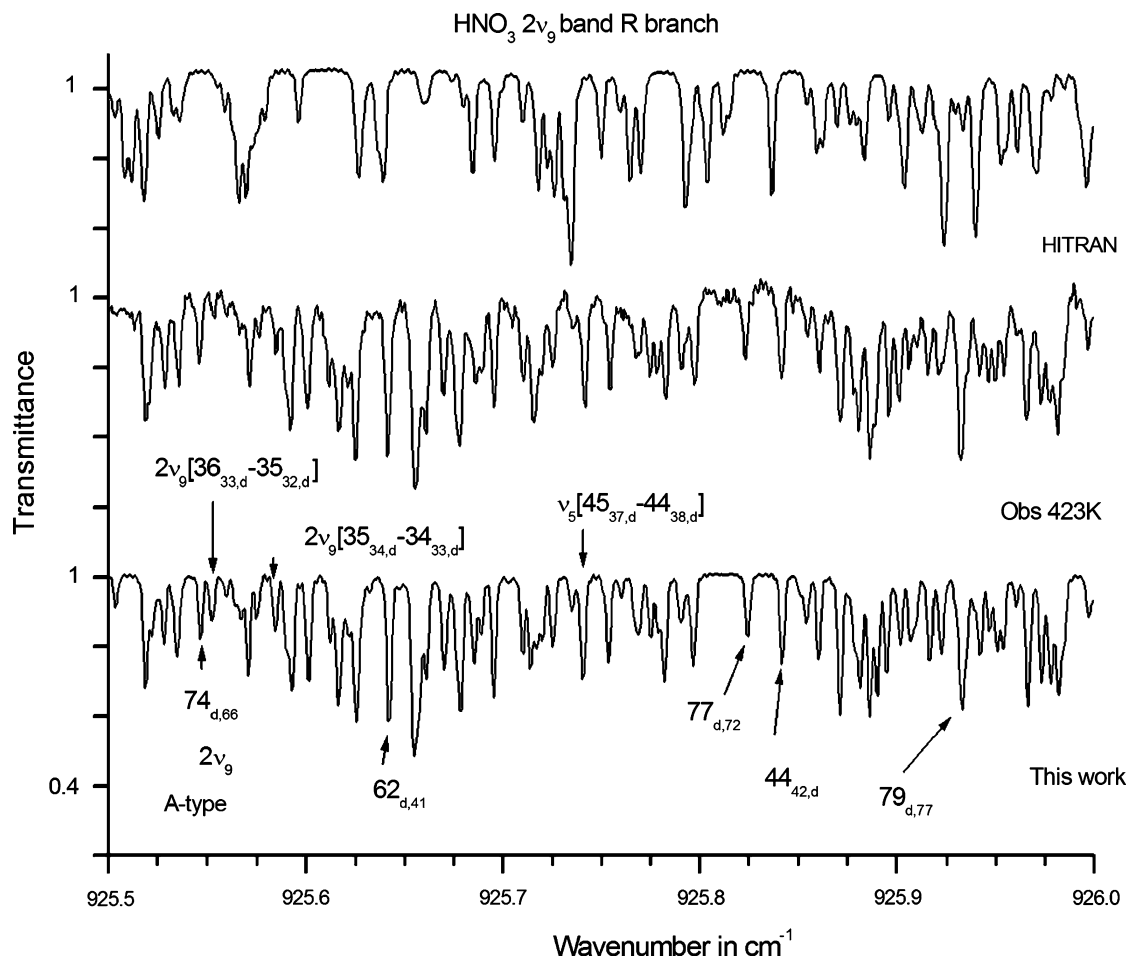


Fig. 2. Part of the R branch of the $2\nu_9$ band at 925.6 cm^{-1} . Upper trace, line by line calculation using the HITRAN line list. Medium trace, observed spectrum recorded at 423 K. Lower trace, line by line calculation (this work). The quality of the new simulation for $2\nu_9$ is excellent both for line positions and intensities, even for transitions involving rather high quantum numbers. Below the lower trace the $J_{K'K''}$ assignments are given for $2\nu_9$ A-type transitions, and d as in Fig. 1 stands for degenerate transitions. In addition two $2\nu_9$ B-type transitions and one ν_5 line are also indicated on the lower trace.

3.1. The torsional splittings in the 9^2 and 5^1 energy levels of HNO_3

The ν_9 mode (torsion of the OH bond relative to the NO_2 moiety) is a large amplitude motion which induces a splitting of the energy levels which increases with increasing excitation in the ν_9 vibrational mode [34]. For the 9^1 state, the torsional splitting is of the order of 2 MHz [35,36]. For the $2\nu_9$ band, the splitting is of the order of $\sim 0.002\text{ cm}^{-1}$ and was first observed by high resolution diode laser spectroscopy [14] but no calculation was performed at that time. More recently, Goyette et al. [20,21] and Petkie et al. [22] performed extensive analyses of the rotational spectra of the ν_5 and $2\nu_9$ bands. Surprisingly enough the torsional splittings were observed not only in the $2\nu_9$ band (as expected) but also in the ν_5 band (which corresponds to the low amplitude NO_2 in plane bending mode). The average observed values are ~ 50 and ~ 35 MHz for the $2\nu_9$ and ν_5 transitions, respectively. Finally, the splitting in the 9^3 vibrational state which is of the order of $\sim 0.060\text{ cm}^{-1}$ was

observed both in the $3\nu_9-\nu_9$ hot band at $11\text{ }\mu\text{m}$ and in the $3\nu_9-\nu_5$ and $3\nu_9-2\nu_9$ hot bands at $22\text{ }\mu\text{m}$ [7].

3.2. The strong resonances coupling the 9^2 and 5^1 energy levels of HNO_3

The 5^1 (NO_2 in plane bend) and 9^2 (first overtone of the ν_9 OH torsion relative to NO_2) states are strongly coupled as evidenced by the following findings:

- At $11\text{ }\mu\text{m}$ the $2\nu_9$ overtone band is almost as strong as the ν_5 fundamental band. More explicitly relative to the ν_5 band the intensity of $2\nu_9$ is in the ratio $\text{Int}(2\nu_9)/\text{Int}(\nu_5) \sim 0.73$ (see Fig. 3). An explanation of such a ratio is that the $2\nu_9$ overtone band which should be weak borrows most of its intensity from the much stronger ν_5 band. In the same way at $22\text{ }\mu\text{m}$ the $\nu_5-\nu_9$ difference band which should be weak is almost as strong as the $2\nu_9-\nu_9$ hot band (see Fig. 1 in [7]).
- As already pointed out, the analysis of mm/submm measurements performed in [20–22], evidenced strong torsional splittings both for the 5^1 and 9^2 rotational

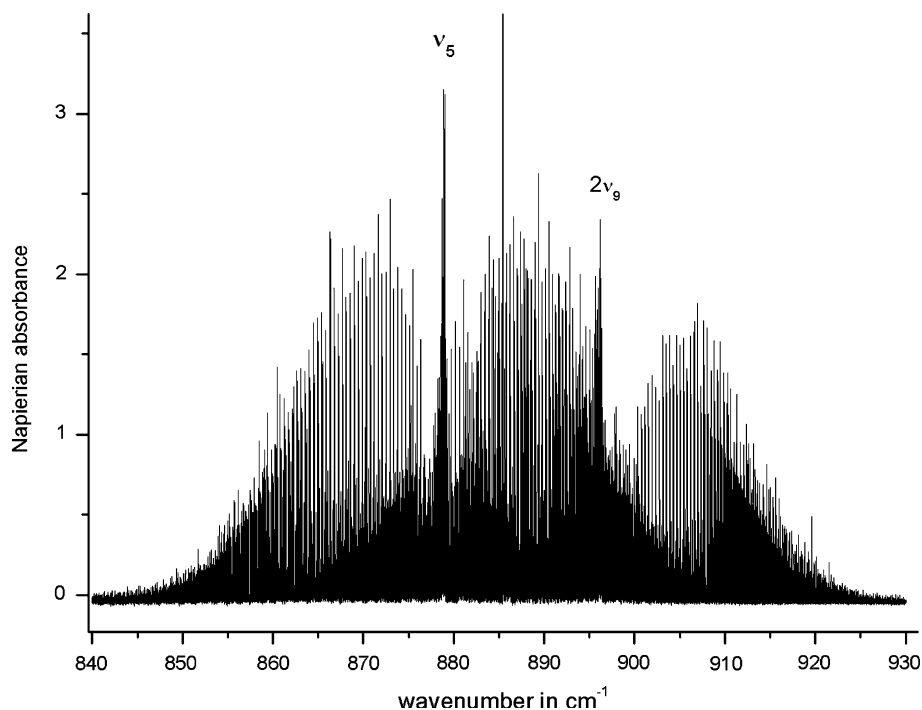


Fig. 3. The $\nu_5/2\nu_9$ bands of HNO_3 recorded at 243.0 K with a spectral resolution of 0.0008 cm^{-1} (1/2MOPD). The spectrum is the average of 280 scans, the temperature stability and homogeneity were better than 0.2 K. The stability of the HNO_3 concentration was assured using the saturated vapor pressure of HNO_3 .

transitions (splitting ($\nu_5 = 1$) ~ 35 MHz and splitting ($\nu_9 = 2$) ~ 50 MHz). A reasonable explanation is that both splittings have their physical origin in the torsional motion of the ν_9 vibrational mode, and that the splitting in $\nu_5 = 1$ is due to the strong mixing of the wavefunctions. As the intensity ratio (~ 0.73) of the $2\nu_9$ overtone band and of the ν_5 fundamental band is more or less equal to the ratio (~ 0.70) of the torsional splittings in 5^1 and 9^2 it is reasonable to conclude, as pointed out in [20–22], that both the transfer (i) of intensity from ν_5 to $2\nu_9$ and (ii) of torsional splitting from 9^2 to 5^1 have their common origin in a strong mixing of the 5^1 and 9^2 wavefunctions. The goal of the present work is to properly model these effects.

4. Experimental data

We have used the extended set of experimental line positions and line intensities [7,18] and millimeter data [20–22] available in the literature as well as new centimeter transitions measured in Kiel and new Fourier transform infrared spectra recorded in Giessen.

4.1. The Kiel centimeter measurements

In Kiel, the measurements in the centimeter-wave range were performed by means of waveguide Fourier

transform microwave spectroscopy. Spectrometers in the ranges 8–18 GHz and 18–26.5 GHz were used, employing sample cells with a rectangular waveguide of length 12 m [37] and a circular waveguide cell of length 36 m [38], respectively. The experiments were carried out at ambient temperature and at gas pressures of ca. 0.5–1.0 Pa. Experimental transition frequencies were obtained from a fit analysis of the transient emission signal, assuming a Voigt profile line function and yielding an accuracy of typically better than 5 kHz (single standard deviation) for the line center frequency, depending on the strength of the line. As it will be pointed out later in the text, the hyperfine structure, which may be important (up to 0.5 MHz) [39] was not accounted for in the present calculation. For this reason only the strongest F-component was considered in the list of experimental measurements.

Table 1 gives the list of the centimeter transitions measured in Kiel.

4.2. Fourier transform spectra

The infrared spectra were recorded using the high-resolution Fourier-transform spectrometer (FTS) Bruker IFS-120 HR at the Physikalisch-Chemisches Institut, Justus-Liebig-Universität Giessen (Germany). The global source inside the Bruker IFS-120 HR and a KBr beamsplitter were used. The scanner speed was adjusted to sample the frequency-stabilized HeNe-laser

Table 1
Microwave transitions in the ν_5 and $2\nu_9$ bands of HNO₃ measured in Kiel

ν (Obs)	ν (Calc)	O–C	J'	K'_a	K'_c	ν'	J''	K''_a	K''_c	ν''
8163.941	8163.903	0.038	21	17	4	99	21	17	5	99
8231.655	8231.691	–0.036	12	10	2	5	12	10	3	5
9492.617	9492.655	–0.038	6	5	1	99	6	5	2	99
9607.790	9607.777	0.013	16	13	3	99	16	13	4	99
9670.916	9671.023	–0.107	21	17	4	5	21	17	5	5
9706.866	9706.823	0.043	25	20	5	99	25	20	6	99
9922.130	9922.521	–0.391	6	5	1	5	6	5	2	5
10331.414	10331.395	0.019	11	9	2	99	11	9	3	99
10953.817	10953.891	–0.074	16	13	3	5	16	13	4	5
10961.260	10961.469	–0.209	34	27	7	99	34	27	8	99
11262.205	11262.117	0.088	29	23	6	99	29	23	7	99
11271.481	11271.549	–0.068	11	9	2	5	11	9	3	5
11598.160	11598.137	0.023	25	20	5	5	25	20	6	5
11752.008	11751.990	0.018	20	16	4	99	20	16	5	99
11817.910	11818.026	–0.116	5	4	1	99	5	4	2	99
12187.930	12188.027	–0.097	5	4	1	5	5	4	2	5
12597.584	12597.993	–0.409	4	4	0	99	4	3	1	99
12637.566	12637.414	0.152	33	29	5	5	33	26	8	99
13308.497	13308.536	–0.039	15	12	3	99	15	12	4	99
13465.769	13465.568	0.201	29	22	8	5	29	23	7	5
13603.157	13603.147	0.010	20	16	4	5	20	16	5	5
13655.789	13655.863	–0.074	10	8	2	99	10	8	3	99
13883.737	13883.667	0.070	24	19	5	99	24	19	6	99
13983.915	13983.872	0.043	4	3	1	99	4	3	2	99
14052.043	14051.735	0.308	37	29	8	5	37	29	9	5
14277.330	14277.430	–0.100	4	3	1	5	4	3	2	5
14606.155	14606.225	–0.070	10	8	2	5	10	8	3	5
14822.700	14822.704	–0.004	15	12	3	5	15	12	4	5
15440.194	15440.184	0.010	33	26	7	5	33	26	8	5
15512.493	15512.443	0.050	5	4	1	99	5	3	2	99
15582.821	15582.901	–0.080	5	4	1	5	5	3	2	5
15810.470	15810.306	0.164	3	2	1	99	3	2	2	99
15860.139	15860.121	0.018	4	3	1	5	4	2	2	5
15954.453	15954.315	0.138	28	22	6	99	28	22	7	99
16203.746	16203.680	0.066	19	15	4	99	19	15	5	99
16212.940	16213.055	–0.115	24	19	5	5	24	19	6	5
16213.687	16213.591	0.096	6	5	1	5	6	4	2	5
16326.779	16326.777	0.002	6	5	1	99	6	4	2	99
16547.671	16547.765	–0.094	3	2	1	5	3	1	2	5
17173.278	17173.269	0.009	9	7	2	99	9	7	3	99
17248.637	17248.652	–0.015	2	1	1	99	2	1	2	99
17577.503	17577.442	0.061	14	11	3	99	14	11	4	99
17994.799	17994.975	–0.176	32	28	5	5	32	28	4	5
18050.676	18050.554	0.122	7	6	1	99	7	5	2	99
18063.564	18063.662	–0.098	9	7	2	5	9	7	3	5
18234.698	18234.710	–0.012	1	0	1	99	0	0	0	99
18287.308	18287.370	–0.062	1	0	1	5	0	0	0	5
18319.532	18319.599	–0.067	19	15	4	5	19	15	5	5
18651.296	18651.273	0.023	38	30	8	5	38	25	13	99
18672.699	18672.618	0.081	28	22	6	5	28	22	7	5
19157.518	19157.609	–0.091	14	11	3	5	14	11	4	5
19280.173	19280.066	0.107	1	1	1	5	0	0	0	5
19288.799	19288.999	–0.2	1	1	1	99	0	0	0	99
20222.522	20222.395	0.127	2	2	1	99	2	1	2	99
20257.126	20257.129	–0.003	2	2	1	5	2	1	2	5
20384.367	20384.300	0.067	2	2	1	99	2	0	2	99
20392.960	20392.841	0.119	2	2	1	5	2	0	2	5
20502.522	20502.408	0.114	8	7	1	5	8	6	2	5
20583.391	20583.609	–0.218	8	6	2	99	8	6	3	99
20644.841	20644.784	0.057	6	6	0	5	6	5	1	5
21145.919	21145.773	0.146	8	7	1	99	8	6	2	99
21209.269	21209.486	–0.217	32	25	7	5	32	25	8	5
21274.406	21274.360	0.046	18	14	4	99	18	14	5	99

Table 1 (continued)

ν (Obs)	ν (Calc)	O – C	J'	K'_a	K'_c	ν'	J''	K''_a	K''_c	ν''
21369.763	21369.596	0.167	8	6	2	5	8	6	3	5
21395.953	21395.826	0.127	6	6	0	99	6	5	1	99
21506.719	21507.316	-0.597	44	35	10	99	44	35	9	99
21666.517	21666.309	0.208	23	18	5	5	23	18	6	5
21731.211	21731.073	0.138	27	21	6	99	27	21	7	99
21738.759	21738.667	0.092	40	31	9	5	40	31	10	5
21818.715	21818.578	0.137	3	3	1	5	3	2	2	5
21877.471	21878.134	-0.663	40	31	9	99	40	31	10	99
21888.991	21888.929	0.062	3	3	1	99	3	2	2	99
22088.832	22088.904	-0.072	13	10	3	99	13	10	4	99
22334.830	22334.724	0.106	3	3	1	5	3	1	2	5
22446.939	22446.754	0.185	3	3	1	99	3	1	2	99
23148.382	23148.624	-0.242	37	30	8	99	37	24	13	99
23517.723	23517.463	0.260	44	33	12	5	44	33	11	5
23532.830	23532.810	0.020	18	14	4	5	18	14	5	5
23583.844	23583.964	-0.120	9	7	2	99	9	6	3	99
23636.703	23636.759	-0.056	13	10	3	5	13	10	4	5
23743.770	23743.783	-0.013	7	5	2	99	7	5	3	99
23744.111	23743.684	0.427	9	7	2	5	9	6	3	5
23797.044	23797.065	-0.021	4	4	1	5	4	3	2	5
23905.047	23905.039	0.008	10	8	2	5	10	7	3	5
24013.847	24013.635	0.212	10	8	2	99	10	7	3	99
24104.735	24104.561	0.174	8	6	2	99	8	5	3	99
24351.412	24351.368	0.044	9	8	1	5	9	7	2	5
24391.391	24391.192	0.199	31	28	3	5	31	28	4	5
24393.570	24393.686	-0.116	7	5	2	5	7	5	3	5
24469.504	24469.628	-0.124	8	6	2	5	8	5	3	5
24880.695	24880.565	0.130	22	17	5	99	22	17	6	99
24905.416	24905.547	-0.131	27	21	6	5	27	21	7	5
25312.886	25312.705	0.181	9	8	1	99	9	7	2	99
25379.855	25379.756	0.099	4	4	1	5	4	2	2	5
25502.112	25502.281	-0.169	7	5	2	99	7	4	3	99
25690.842	25690.731	0.111	4	4	1	99	4	2	2	99
25867.986	25868.062	-0.076	11	9	2	99	11	8	3	99
25917.519	25917.532	-0.013	7	5	2	5	7	4	3	5
26086.963	26086.738	0.225	7	7	0	5	7	6	1	5
26410.187	26410.252	-0.065	6	4	2	99	6	4	3	99
26414.359	26414.083	0.276	5	5	1	5	5	4	2	5
26531.632	26531.495	0.137	35	29	6	5	35	29	7	5

ν (Obs) and ν (Calc): experimental and calculated line positions in MHz.

O – C: Observed – Calculated difference in MHz.

J' , K'_a , K'_c , J'' , K''_a , K''_c : Upper and lower state rotational quantum numbers ν' , ν'' : Upper and lower state vibrational quantum numbers; 99 and 5 stand for 9² and 5¹ respectively.

at 40 kHz. The input aperture was limited to 1.3 mm to avoid self-apodization for the high spectral resolution of all the spectra ($1/(2\text{MOPD})=0.0008\text{ cm}^{-1}$, MOPD: maximum optical path difference) [40]. The use of an optical bandpass filter limited the spectral range to the folding limits of 718 and 1436 cm^{-1} , thus covering simultaneously the ν_3 , ν_4 , ν_5 , and $2\nu_9$ bands of HNO_3 . All spectra were recorded with the FTS evacuated to about 10^{-2} mbar to avoid residual water absorption. For spectral calibration, a high-resolution spectrum of gaseous N_2O was recorded. The calibration was performed using 79 standard reference line positions from NIST [41] leading to an RMS wavenumber uncertainty of 0.00011 cm^{-1} . All line positions were determined using the OPUS peakfinder routine.

The temperature-stabilized absorption cell has a total length between the windows (made of polyethylene) of 302 cm and is installed between the interferometer chamber and the separate chamber for the copper-doped germanium detector (kept at liquid helium temperature). The temperature of the absorption cell is regulated using a flow of gaseous nitrogen evaporating from a dewar with liquid N_2 at 77 K, together with heating resistance wires. The temperature is monitored by 16 temperature sensors installed around the cell and logged and controlled by a personal computer. More details of the temperature-controlled cell are given in [42]. The temperature stability and homogeneity was better than 0.2–0.5 K for the spectra at room temperature and better than 0.2–1.0 K for the spectra at lower and higher temperatures.

Pure samples of HNO₃ were synthesized immediately before filling of the absorption cell using a vacuum-line connected to a small Pyrex bulb, where liquid H₂SO₄ (>99%) was dropped onto pure KNO₃ (Aldrich, 99.99%). The pressure was monitored using a calibrated capacitive pressure transducer (MKS Baratron). The values varied between 0.003 mbar at 210 K and 1.30 mbar at 423 K. No attempt was made to determine the concentrations of HNO₃ inside the cell because of the low pressure values at temperatures at and below ambient and due to the thermal decomposition of HNO₃ at higher temperatures.

Particular care was paid to the stability of the amount of HNO₃ while recording high-resolution scans. To minimize HNO₃ decomposition, the KBr windows were coated by thin polyethylene foil (cling film). Also for this purpose, spectra were recorded in blocks of 10, 20, 30 or 50 scans (depending on the temperature). After passivation of the absorption cell for several days with gaseous HNO₃, the decomposition at room temperature was observed to be less than 1% over several hours. However, at the highest temperature recorded (423 K), the decomposition was about 50% over 18 h, probably due to thermal dissociation of HNO₃. The decomposition products observed in the spectra were H₂O, NO₂, and N₂O.

High-resolution absorption spectra of HNO₃ were recorded at sample temperatures of 210.0, 243.0, 299.7, 347.5, and 423.2 K. The spectra at 210 and 243.0 K were recorded using the saturated vapour pressure of HNO₃ in the absorption cell (0.003 and 0.041 mbar, respectively), which assured a very high stability of the column density of gaseous HNO₃ inside the cell during the experiments. Generally, 10–20 high-resolution blocks were recorded over a period of 12–24 h for each sample temperature. The resulting spectra show a very high signal/noise ratio (larger than 100 for the Q branch around 879 cm⁻¹ when looking at the Napierian absorbance, see Figs. 1–3). To the best of our knowledge, these are the first high-resolution absorption spectra of HNO₃ recorded in the laboratory for such a large range of temperatures, and it is important to stress the fact that these new experiments also cover stratospheric temperatures.

5. Analyses of the infrared spectra

According to symmetry considerations, both the ν_5 and $2\nu_9$ bands are hybrid (with both *A*- and *B*-type components). In fact, for ν_5 only the *A*-type component was observed and for $2\nu_9$ the *A*-type component is much stronger than the *B*-type one. For *A*-type transitions, the strongest lines involve [*J*, *K_a*, *K_c*] rotational levels with $K_a \ll K_c \sim J$ in the P and R branches while in the Q branches mainly transitions with $K_c \ll K_a \sim J$ are ob-

servable. However, these Q branches are largely congested making the assignments rather difficult. To circumvent this problem we have then extended the analysis [7] of the ν_5 – ν_9 and $2\nu_9$ – ν_9 hot bands located at 22 μm which are *C*-type bands. Indeed for these *C*-type bands, the strongest lines in the P- and R-branches are those with $K_c \ll K_a \sim J$.

This analysis was performed in two steps, first extrapolating the results of [16] and second using the theoretical model described in the next section. In total 12 853 lines (3971 and 8882 at 22 and 11 μm , respectively) were assigned. They were added to the ground state energy levels [43] leading to the determination of 1987 and 2142 energy levels for the 5¹ and 9² vibrational states, respectively.¹ The set of energy levels is complete up to $J = 33$ for both 5¹ and 9², and the maximum J and K_a values are $J = 79$ and $K_a = 43$. Therefore, one can say that significant progress were made as compared to what was obtained in [16] since at that time only 2334 energy levels with $J \leq 65$ and $K_a \leq 40$ were obtained for {5¹, 9²}.

6. Line positions calculations

6.1. Hamiltonian matrix

As already said, the energy levels calculation for the {5¹, 9²} interacting states must account for two effects: – the torsional splittings which affect both ν_5 and $2\nu_9$ rotational transitions, – the very strong Fermi and Coriolis resonances.

Therefore, the Hamiltonian matrix used in this work to compute the 5¹ and 9² energy levels takes the general form which is given in Table 2.

The H_v^{ROT} rotational operator. For each of the 5¹ and 9² states, the H_v^{ROT} rotational operators includes XZ_v non-orthorhombic terms in addition to the Watson's operator written in an *I'* representation with a *A*-type reduction [44]. These non-orthorhombic terms in XZ_v which are symmetry allowed (*xz* is the molecular plane) are usually removed for *C_s*-type molecules by rotational contact transformations [44], leading to an *A*-type (or *S*-type) Watson type reduced Hamiltonian. Adding these XZ_v terms means that the system of reference axes differs from the inertial axes. It is worth noticing that such terms were also necessary to reproduce the energy levels of another *C_s*-type molecule HDCO [45,46].

The H_v^{TORS} torsional operator. To account for the torsional effects, we used the IAM method. This method was originally developed for the water dimer [47–49], and later on was also used to account for the torsional

¹ The list of assigned transitions and the corresponding list of energy levels together with their errors has been deposited as supplementary material at the Journal of Molecular Spectroscopy. It is also available from A. Perrin.

Table 2
Hamiltonian matrix for the $\{5^1, 9^2\}$ interacting vibrational states of HNO₃

	5 ¹	9 ²
5 ¹	$H_{5,5}$	c.c
9 ²	$H_{99,5}$	$H_{99,99}$

v-diagonal operators: $H_{vv} = H_v^{\text{ROT}} + H_v^{\text{TORS}}$

Rotational operator: $H_v^{\text{ROT}} = {}^w H_v^{\text{ROT}} + XZ_v$

${}^w H_v^{\text{ROT}} = E_v + A_v J_z^2 + B_v J_x^2 + C_v J_y^2 - \Delta_K^v J_z^4 - \Delta_{JK}^v \mathbf{J}^2 J_z^2 - \Delta_v^v \mathbf{J}^4 - 2\delta_v^v \mathbf{J}^2 J_{xy}^2 - \delta_K^v \{J_z^2, J_{xy}^2\} + \dots$

$XZ_v = h_0^v \{J_x, J_z\} + h_z^v \{J_x, J_z, J_z^2\} + h_v^v \mathbf{J}^2 \{J_x, J_z\} \dots$ (non-orthorhombic terms)

Torsional operator: $H_{99}^{\text{TORS}} = \{ {}^{\text{IAM}} W^{\text{TORS}}, {}^{\text{IAM}} H_R^{\text{TORS}} \}$

$\langle JK'\gamma' | H_{99}^{\text{TORS}} | JK\gamma \rangle = \sum_{K''\gamma''} \{ \langle JK'\gamma' | {}^{\text{IAM}} W^{\text{TORS}} | JK''\gamma'' \rangle, \langle JK''\gamma'' | {}^{\text{IAM}} H_R^{\text{TORS}} | JK\gamma \rangle \}$

(for $K' \neq 0$ and $K'' \neq 0$):

$\langle JK'\gamma' | {}^{\text{IAM}} W^{\text{TORS}} | JK''\gamma'' \rangle = (-1)^{K'} \left(\cos((K' + K'')\varphi) d_{K',K''}^{(J)}(\theta) + \gamma'' \cos((K' - K'')\varphi) d_{K',-K''}^{(J)}(\theta) \right)$

(for $K' \neq 0$) $\langle JK'\gamma' | {}^{\text{IAM}} W^{\text{TORS}} | JK'' = 0 \gamma'' = +1 \rangle = (-1)^{K'} \sqrt{2} \cos(K'\varphi) d_{K',0}^{(J)}(\theta)$

(for $K'' \neq 0$) $\langle JK' = 0 \gamma' = 0 | {}^{\text{IAM}} W^{\text{TORS}} | JK''\gamma'' \rangle = \sqrt{2} \cos(K''\varphi) d_{0,K''}^{(J)}(\theta)$

(for $K' = K'' = 0$) $\langle JK' = 0 \gamma' = +1 | {}^{\text{IAM}} W^{\text{TORS}} | JK'' = 0 \gamma'' = +1 \rangle = d_{0,0}^{(J)}(\theta)$

with : $\theta = \theta_0 + \theta_J J(J+1)$

${}^{\text{IAM}} H_R^{\text{TORS}} = E_0^{\varphi\theta} + E_J^{\varphi\theta} \mathbf{J}^2 + E_z^{\varphi\theta} J_z^2 + E_{xy}^{\varphi\theta} J_{xy}^2 + \dots$

v-off-diagonal operators: $H_{99,5} = F + C$ (Fermi and Coriolis)

$F = F_0 + F_J \mathbf{J}^2 + F_z J_z^2 + F_{xy} J_{xy}^2 + F_{xy,z} \{J_{xy}^2, J_z^2\} + 2.F_{xy,J} J_{xy}^2 \mathbf{J}^2 + \dots$

$C = C_y i J_y + C_{xz} \{J_x, J_z\} + C_{xz,J} \{J_x, J_z\} \mathbf{J}^2 + C_{xz,z} \{J_z^2, \{J_x, J_z\}\} + \dots$

with: c.c. complex conjugate; $\{A, B\} = AB + BA$; $J_{xy}^2 = J_x^2 - J_y^2$

$|JK\gamma\rangle =$ Wang symmetry adapted basis: ($\gamma = \pm 1$) and $|JK\gamma\rangle = 1/\sqrt{2}(|JK\rangle + \gamma|J-K\rangle)$; $|JK = 0 \gamma = +1\rangle = |J0\rangle$

effects in HNO₃: firstly for the analysis of a first set of ν_5 and $2\nu_9$ microwave transitions [30], and then for an extended analysis of the rotational transitions in the ν_9 state of HNO₃ [36].

In this approach the z -molecular axis of the Hamiltonian does not coincide with the direction of the torsional angular momentum and the so-called ‘‘torsional operator’’ accounts for the Coriolis coupling between the angular momentum generated by the large amplitude motion and the overall rotation of the molecule. This coupling leads to a rotational dependence of the tunneling splitting (H_{99}^{TORS} operators in Table 2). H_{99}^{TORS} is written as an anticommutator of an expansion of rotational operators ${}^{\text{IAM}} H_R^{\text{TORS}}$ and of the matrix elements ${}^{\text{IAM}} W^{\text{TORS}} = D^{(J)}(\chi', \theta', \varphi')_{K,K'}$ of the $D(\chi', \theta', \varphi')$ Wigner’s operators [50].

$$D^{(J)}(\chi', \theta', \varphi')_{K,K'} = \langle JK | D(\chi', \theta', \varphi') | JK' \rangle. \quad (1)$$

For nitric acid, the tunneling motion consists of a 180° rotation of the OH bond. During this motion, HNO₃ goes from one planar configuration to another one, with an intermediate configuration possessing a plane of symmetry. This motion is analogous to the ‘‘1 → 4’’ tunneling motion of water dimer and the $D^{(J)}(\chi', \theta', \varphi')_{K,K'}$ functions take a rather simple form because of symmetry relations involving the three angles χ' , θ' , and φ' , [30]. In fact, since

$\chi' = \varphi' + 180^\circ$, only two angles, namely θ and φ are relevant: these angles describe the net rotation that the IAM coordinate system undergoes along the tunneling path as it twists and turns to achieve cancellation of the internal angular momentum generated by the tunneling motion. In the present study, the OH bond is defined as the rotor and the NO₂ moiety as the frame. More explicitly, the angle 2φ corresponds to the backward rotation of the whole molecule after the 180° tunneling motion of the OH rotor,² [47]:

$$2\varphi = 180^\circ \frac{I_{\text{rotor}}}{I_{\text{rotor}} + I_{\text{frame}}}. \quad (2)$$

The angle θ represents the change in the z -quantization axis during the 180° tunneling motion of OH.

As in [49] the expansion of ${}^{\text{IAM}} H_R^{\text{TORS}}$ (Table 2) includes, together with a constant term $E_0^{\varphi\theta}$, higher order operators of the form $E_J^{\varphi\theta} \mathbf{J}^2$, $E_z^{\varphi\theta} J_z^2$, and $E_{xy}^{\varphi\theta} J_{xy}^2$. Also as in [49] it proved useful to use a J -dependent description for θ :

$$\theta(J) = \theta_0 + \theta_J J(J+1). \quad (3)$$

² In [22], by convention the NO₂ moiety is defined as the rotor and the OH bond as the frame and $\rho = (I_{\text{rotor}})/(I_{\text{rotor}} + I_{\text{frame}})$ was held fixed at the value $\rho = 0.978793$ (ρ corresponds to $1 - 2\varphi/180^\circ$ in the present study).

The operators off-diagonal in v . Due to symmetry considerations, both Fermi- and C-Coriolis type resonances are to be considered in the off-diagonal operators $H_{99,5}$ (see Table 2).

Finally, and as in [20–22], the quadrupole hyperfine structure of HNO_3 [39] which was easily observed in some of the centimeter transitions measured in Kiel, was not taken into account in the present calculation: depending on the transitions, this hyperfine structure can lead to splittings up to 0.5 MHz, which are negligible in infrared spectra. The data were weighted accordingly.

6.2. Results

The least squares fit involves:

- 4129 upper state infrared energy levels
- The set of millimeter and submillimeter transitions collected in [20–22],
- 102 additional new centimeter transitions which were measured in Kiel (Table 1).

Weights used in the fit were taken equal to the inverse squares of the experimental uncertainties i.e., 10^{-4} cm^{-1} for the isolated infrared transitions, as given in the literature for the millimeter and submillimeter data and 0.1 MHz for the centimeter transitions.

The fit was very satisfactory as can be seen from the statistical analyses given in Table 3 and the obtained standard deviations: $0.63 \times 10^{-3} \text{ cm}^{-1}$ for the infrared levels and 0.15 MHz for the microwave transitions. The corresponding Hamiltonian constants are given in Table 4 together with their uncertainties. It is worth noticing that these uncertainties are statistical uncertainties and do not account for systematic errors. In particular it is estimated that the accuracy on the band centers is not better than 0.0003 cm^{-1} . On the other hand the number of digits given for each constant is necessary to calculate the transitions with the right precision.

Table 3
Statistical analysis of the results of the energy level calculation

	5^1	9^2
(A) Infrared levels^a		
Number of levels:	1987	2142
$0 \leq \delta \leq 0.5 \times 10^{-3} \text{ cm}^{-1}$	90.1%	80.1%
$0.5 < \delta \leq 1.0 \times 10^{-3} \text{ cm}^{-1}$	8.4%	15.8%
$1.0 \leq \delta \leq 3.0 \times 10^{-3} \text{ cm}^{-1}$	1.5%	4.1%
Standard deviation (10^{-3} cm^{-1}):	0.63	
(B) cm and mm/submm transitions		
	ν_5 and $2\nu_9$	
Number of transitions:	2414	
$0 \leq \delta \leq 0.2 \text{ MHz}$	84.8%	
$0.2 < \delta \leq 0.5 \text{ MHz}$	14.3%	
$0.5 < \delta \leq 0.8 \text{ MHz}$	0.9%	
Standard deviation (MHz):	0.15	

^a $\delta = |E_{\text{obs}} - E_{\text{calc}}|$.

6.3. Discussion

In this section we discuss problems concerning the signs of some Hamiltonian constants, the definition of the angles involved in the torsional operators and we compare the present results with previous ones.

Absolute signs of the Hamiltonian constants and definition of the torsional angles. Important pieces of information which may or may not be obtained from a least squares fit calculation are the absolute signs of the parameters. In the present case, they are important for the physical significance of the h_5 and h_{99} non-orthorhombic constants and of the torsional parameters.

As usual, the signs of all the parameters appearing in the orthorhombic part of the rotational Hamiltonians (i.e., the Watson A -type expansions) of the two states under study are obtained from the fit.

The torsional operators which are to be considered appear in the 9^2 vibrational block (see Table 2). Accordingly, the signs for all the constants appearing in the expansion of ${}^{\text{IAM}}H^{\text{TORS}}$ are determined unambiguously since H_{99}^{TORS} has matrix elements in the same 9^2 diagonal part of the Hamiltonian as the Watson rotational Hamiltonian. In this way a negative value was determined from the fit for $E_0^{\varphi\theta}$ and this is consistent with predictions from the torsional potential of HNO_3 [7].

The situation is completely different for the signs of the constants occurring in the Fermi and Coriolis operators or in the XZ_{vv} non-orthorhombic parts of the rotational operators, as well as for the angles φ and θ . More precisely, the question concerns the signs of the lower order constants F_0 , C_{xz} , h_0^5 , h_0^{99} , and the θ_0 angle involved in the expansion of the corresponding operators since the signs of the higher order constants relative to the signs of the lower order constants are determined through the fit.

As explained in [45,46] the eigenvalues obtained through the diagonalization of the Hamiltonian matrix remain unchanged when performing:

- (i) a change of sign of the q_5 normal mode.

$$q_5 \Rightarrow -q_5, \quad (4)$$

which leads to a simultaneous change of signs for F_0 and C_{xz} only.

$$C_{xz} \Rightarrow -C_{xz} \text{ and } F_0 \Rightarrow -F_0 \quad (5)$$

- (ii) a change of direction of two of the three inertial axes

$$(a, b, c) \Rightarrow (a, -b, -c) \text{ or } (a, b, c) \Rightarrow (-a, b, -c), \quad (6)$$

which leads to the following changes of signs for the constants and to the following changes for the φ and θ_0 angles:

$$C_{xz} \Rightarrow -C_{xz} \text{ and } h_0^5 \Rightarrow -h_0^5 \text{ and } h_0^{99} \Rightarrow -h_0^{99}, \text{ and } \varphi \Rightarrow 180^\circ \pm \varphi \text{ or } \theta_0 \Rightarrow -\theta_0 \quad (7)$$

Table 4

Vibrational energies, rotational, torsional, and interacting constants for the $\{5^1, 9^2\}$ vibrational states of HNO_3

	5^1	9^2
Vibrational energies and rotational constants (in cm^{-1})		
E_V	886.2286661(9)	889.3270731(10)
A	0.4323881958(35)	0.4325936182(30)
B	0.4048708585(22)	0.3991881084(18)
C	0.2079957854(49)	0.2084354775(43)
Δ_K	$0.14366657(480) \times 10^{-6}$	$0.1189942(110) \times 10^{-6}$
Δ_{JK}	$-0.7754306(250) \times 10^{-7}$	$-0.5422397(330) \times 10^{-7}$
Δ_J	$0.28898326(450) \times 10^{-6}$	$0.28538164(450) \times 10^{-6}$
δ_K	$0.30653136(970) \times 10^{-6}$	$0.2697388(100) \times 10^{-6}$
δ_J	$0.12205071(140) \times 10^{-6}$	$0.120349485(870) \times 10^{-6}$
H_K	$-0.21146(180) \times 10^{-11}$	$-0.75157(200) \times 10^{-11}$
H_{KJ}	$0.27128(130) \times 10^{-11}$	$0.109519(180) \times 10^{-10}$
H_{JK}		$-0.334334(620) \times 10^{-11}$
h_K	$0.61472(170) \times 10^{-11}$	$0.42100(170) \times 10^{-11}$
h_{KJ}	$-0.169628(320) \times 10^{-11}$	$-0.134318(110) \times 10^{-11}$
	5^1	9^2
Constants involved in the non-orthorhombic operators (in cm^{-1})		
$\{J_x, J_z\}$	h_0^5 $-0.67541760(130) \times 10^{-2}$	h_0^{99} $-0.54080521(180) \times 10^{-2}$
$\{J_z^2, \{J_x, J_z\}\}$		h_z^{99} $0.261576(140) \times 10^{-7}$
$J^2\{J_x, J_z\}$	h_J^5 $0.17803(170) \times 10^{-7}$	h_J^{99} $-0.3500924(820) \times 10^{-7}$
Torsional constants (for 9^2 only)		
(in $^\circ$)	(in cm^{-1})	
θ_0 0.97852(160)	$E_0^{\varphi\theta}$ $-1.436736(640) \times 10^{-3}$	
θ_J $-0.0002649(130)$	$E_J^{\varphi\theta}$ $-0.6851(140) \times 10^{-7}$	
ϕ 1.91197(120)	$E_z^{\varphi\theta}$ $0.5775(230) \times 10^{-7}$	
	$E_{xy}^{\varphi\theta}$ $-0.29049(720) \times 10^{-7}$	
Fermi	Coriolis	
Interaction constants (in cm^{-1})		
F_0 8.530188808(620)	C_{xz} $0.1060086(120) \times 10^{-3}$	
F_J $-0.27075276(110) \times 10^{-3}$	$C_{xz,J}$ $-0.25620(100) \times 10^{-8}$	
F_z $0.26408123(290) \times 10^{-3}$		
F_{xy} $-0.23397493(210) \times 10^{-3}$		
$F_{xy,J}$ $-0.208023(600) \times 10^{-9}$		
$F_{xy,z}$ $0.1235483(310) \times 10^{-7}$		

The quoted errors are one standard deviation.

Therefore, one has to use conventions. We have chosen:

$$F_0 > 0, C_{xz} > 0, 0 \leq \varphi \leq 90^\circ. \quad (8)$$

These constraints correspond to:

- (i) Choosing a q_5 mode of vibration leading to a positive value for F_0 .
- (ii) Defining the (x, y, z) and (a, b, c) systems of axes as given in Fig. 4, leading to a positive value for C_{xz} .
- (iii) Choosing OH as the rotor performing a $+180^\circ$ (positive) torsional tunneling motion around NO_2 (see Fig. 4), which corresponds to $0 \leq \varphi \leq 90^\circ$.

As a consequence of these choices, the signs of the h_0^5 , h_0^{99} , and θ_0 constants are determined from the least squares fit.

Axis switching effects. The reference system of axes in the 5^1 and 9^2 vibrational states are clearly different from the inertial axis system (a, b, c) because of the existence of XZ_v non-orthorhombic terms in the v -diagonal part of the rotational Hamiltonian. As a consequence, according to the conventions which are given in Fig. 4, the

(z_v, x_v, y_v) reference system of axes for each of the 5^1 and 9^2 vibrational states can be obtained from the (a, b, c) inertial system by an anticlockwise rotation around the c -axis of an angle α_v (see Fig. 4):

$$\alpha_v \approx 1/2 \text{atan}\left(-2h_0^v / (A_v - B_v)\right). \quad (9)$$

According to the values of the h_0^v , A_v , and B_v constants (Table 4), these angles are $\alpha_5 \approx 13.08^\circ$ and $\alpha_{99} \approx 8.97^\circ$ for the 5^1 and 9^2 states, respectively. This is a strong effect since α_5 and α_{99} are only slightly smaller than the angle $\angle 14.78^\circ$ between the a -inertial axis and the N–O bond (see Fig. 4), as it can be calculated from the average structure of HNO_3 [51]. As we will see in the next chapter, this effect has to be considered properly if reliable line intensities are to be calculated.

Coriolis parameters. In the present work the Coriolis term in $\mathbf{i} * \mathbf{J}_y$ could not be determined. This is understandable since a large part of the Coriolis interactions between the 5^1 and 9^2 energy levels is already accounted

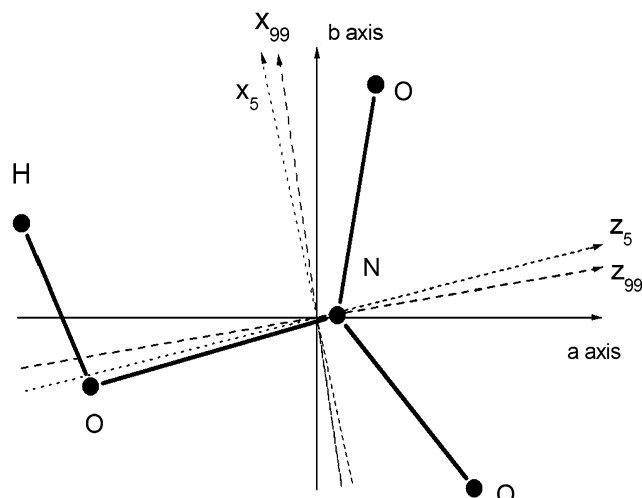


Fig. 4. Structure of the HNO_3 molecule and definition of the axes. Because of the existence of non-orthorhombic terms in the v -diagonal parts of the Hamiltonian, the (x_5, y_5, z_5) and (x_{99}, y_{99}, z_{99}) systems of reference axes for 5^1 and 9^2 , respectively, differ significantly from the (b, c, a) inertial system.

for by the α_5 and α_{99} axis switching angles. An analogous behavior was observed in [22].

The φ and θ_0 torsional parameters. The value of φ determined in this work $\varphi = 1.91197(120)^\circ$ agrees with the value $^{\text{Calc}}\varphi \sim 1.84^\circ$ calculated using Eq. (2) and the structural parameters of [51], as well as with the values $\varphi_9 = 1.9053(2300)^\circ$ and $\varphi_{5,99} = (\varphi_5 + \varphi_{99})/2 = 1.9042^\circ$ obtained for the 9^1 state [36] and for the 5^1 and 9^2 states [30] showing the consistency of the various calculations.

On the other hand, the value derived in this work for the θ_0 angle ($\theta_0 = 0.9785(160)^\circ$) differs very significantly from those obtained in [36] $\theta_9 = 22.637^\circ$ for 9^1 and in [30] $\theta_{5,99} = (\theta_5 + \theta_{99})/2 = 22.80^\circ$ for 5^1 and 9^2 . Such a difference can be expected since the reference system of axes they used (classical inertial) is totally different from the one used in this work: the (z_5, x_5, y_5) and (z_{99}, x_{99}, y_{99}) reference system of axes for 5^1 and 9^2 are indeed obtained from the inertial system of axes through rotations $C_y(\alpha_v)$ of α_v angles around the y axis ($\alpha_5 \approx 13.08^\circ$ and $\alpha_{99} \approx 8.97^\circ$). To compare precisely the results, it is necessary to use the 3×3 direction cosine matrices S^{-1} ($\chi' = \varphi' + 180^\circ, \theta', \varphi'$) [47,52], which describe the tunneling motion in the approach of [30] ${}^{(C)}S^{-1}(C\chi' = {}^C\varphi_{5,99} + 180^\circ, {}^C\theta_{5,99}, {}^C\varphi_{5,99})$ and in the present study ${}^{(\text{PS})}S^{-1}(\chi' = \varphi + 180^\circ, \theta_0, \varphi)$. For that we define α_0 as the average angle of the rotation $C_y(\alpha_0)$ allowing one to obtain the reference axis system for the upper states from the inertial axis system of axis:

$$\alpha_0 \sim (\alpha_5 + \alpha_{99})/2 \approx 11.0^\circ. \quad (10)$$

Then in the inertial axis system ${}^{(\text{PS})}S^{-1}(\chi' = \varphi + 180^\circ, \theta_0, \varphi)$ transforms as:

$${}^{(\text{PS})}'S^{-1} = C_y(\alpha_0) * {}^{(\text{PS})}S^{-1}(\chi' = \varphi + 180^\circ, \theta_0, \varphi) * C_y(\alpha_0)^{-1}. \quad (11)$$

Using the numerical values quoted above for the various angles one gets:

$${}^{(C)}S * {}^{(\text{PS})}'S^{-1} = \begin{pmatrix} 1.000 & -0.0015 & 0.0037 \\ 0.0015 & 1.0000 & 0 \\ -0.0037 & 0 & 1.000 \end{pmatrix}. \quad (12)$$

This shows clearly that the approach of [30] and the approach used in this paper are physically equivalent. The product of the two direction cosine matrices is indeed an almost unitary matrix.

7. Line intensities

This section is devoted to the description of the method which has been used to calculate accurately the line intensities. More precisely, for the modeling of the line intensities it proved necessary to account properly for the axis switching effects. For the experimental data we used the extensive set of individual line intensities measured recently in [18] and it is already worth noticing that the calculations demonstrate that the internal consistency of these experimental data is excellent.

7.1. Axis switching effect

For the line intensity calculation, we face the problem that the reference axes are different in the upper $\{5^1, 9^2\}$ excited states and in the ground vibrational state. For $\{5^1, 9^2\}$ indeed the reference axes z and x differ substantially from the a and b inertial axes.³ On the contrary for the ground vibrational state the wave functions are calculated using a standard I' Watson A -type Hamiltonian and the reference axes are the a , b , and c inertial axes of the molecule [43]. When the axis switching effect is not considered, the experimental spectrum is poorly modeled. This can be seen in Figs. 5 and 6 where the line intensity calculation leads to the computation of unrealistic strong B -type transitions even when using a pure A -type transition moment operator for the ν_5 band. Similar effects are also observed for the $\nu_5-\nu_9$ and $2\nu_9-\nu_9$ hot bands at $22\mu\text{m}$: when neglecting the axis switching effects and using for the 9^1 vibrational state the Watson's type parameters of [43] non-existing forbidden ($\Delta K_a = \text{even}$, $\Delta K_c = \text{even}$) transitions are computed for these pure C -type bands [53].

Such a situation has already been encountered for acetylene [54]: as the geometry of the molecule is different in the \tilde{A} upper electronic state and in the ground electronic state the intensities were calculated using a special tensorial approach which accounts for the axis

³ We would like to emphasize that such a problem was not encountered in our previous line intensity calculation [17] since at that time the 5^1 and 9^2 energy levels were calculated in the (a, b, c) inertial reference axes system.

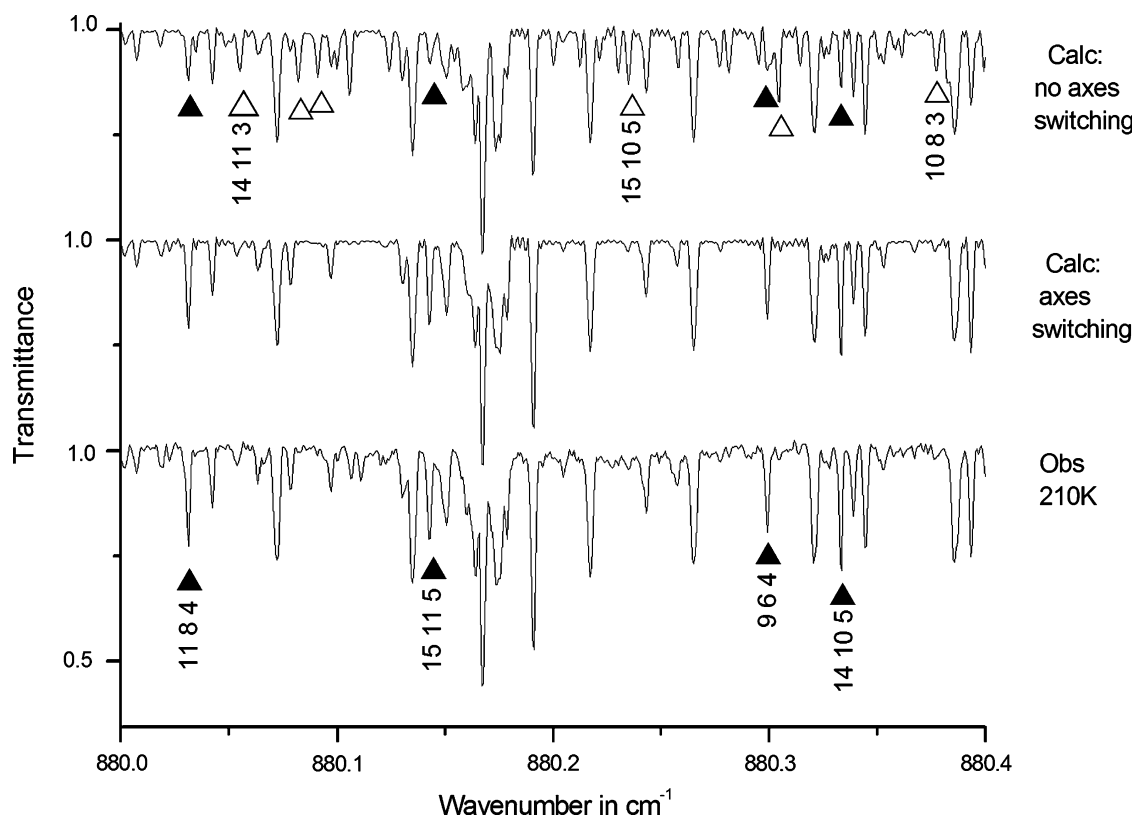


Fig. 5. Part of the spectrum in the 880 cm^{-1} region. The lower trace is the observed spectrum recorded at 210 K. Both medium and upper traces were calculated using the same set of Hamiltonian and transitions moments constants (see Table 3 and Table 5, and [43]). It is clear that the axis switching effect has to be taken into account. Lines indicated by a solid (resp. open) triangle are A -type transitions (resp. B -type) of the ν_5 band which are clearly not properly calculated when the axis switching effect is not considered.

switching effect [54–56]. Because we are facing a similar problem, this formalism was also adopted for the present study of HNO_3 .

The intensity of a line [57,58] is given (in $\text{cm}^{-1}/(\text{molecule cm}^{-2})$) by:

$$k_{\tilde{\nu}}^N = \frac{8\pi^3 \tilde{\nu}}{4\pi\epsilon_0 3hcZ(T)} \left(1 - \exp\left(-\frac{hc\tilde{\nu}}{kT}\right)\right) \exp\left(-\frac{hcE_A}{kT}\right) R_A^B, \quad (13)$$

where A and B are, respectively, the lower and upper levels of the transition, $\tilde{\nu} = (E_B - E_A)/hc$ is the wavenumber of the transition and $Z(T)$ is the total partition function:

$$Z(T) = Z_{\text{vib}}(T)Z_{\text{rot}}(T) \quad (14)$$

(In the following, we use:

$$\begin{aligned} Z_{\text{vib}}(210\text{ K}) &= 1.08679, \\ Z_{\text{rot}}(210\text{ K}) &= 16366 \quad \text{and therefore} \quad Z(210\text{ K}) = 17787, \\ Z_{\text{vib}}(296\text{ K}) &= 1.29952, \\ Z_{\text{rot}}(296\text{ K}) &= 27380 \quad \text{and therefore} \quad Z(296\text{ K}) = 35581, \\ Z_{\text{vib}}(299\text{ K}) &= 1.30972, \\ Z_{\text{rot}}(299\text{ K}) &= 27796 \quad \text{and therefore} \quad Z(299\text{ K}) = 36405, \\ Z_{\text{vib}}(423\text{ K}) &= 1.93163, \\ Z_{\text{rot}}(423\text{ K}) &= 46554 \quad \text{and therefore} \quad Z(423\text{ K}) = 89925. \end{aligned}$$

Finally, R_A^B is the square of the matrix element of the transformed transition moment operator μ'_Z :

$$R_A^B = |\langle v', J'K'_aK'_c | \mu'_Z | 0, J''K''_aK''_c \rangle|^2, \quad (15)$$

where μ'_Z is the transformed dipole moment operator [57,58]. The calculation of the matrix elements of μ'_Z is extensively described in [57], and only the details relevant for this study are given here.

μ'_Z can be expanded as

$$\mu'_Z = \sum_{v' \in B'} |0\rangle^v \mu'_Z \langle v'|, \quad (16)$$

where v' belongs to the upper $B' = \{5^1, 9^2\}$ polyad of interacting states. For symmetry reasons, both A -type and B -type transitions can in principle be observed for the ν_5 and $2\nu_9$ bands. Therefore, up to the first order, the transition moment operator can be written as:

$${}^v \mu_Z = \varphi_z {}^v \mu_z^1 + \varphi_x {}^v \mu_x^1 + \dots, \quad (17)$$

where φ_z and φ_x stand for the direction cosines ϕ_z and ϕ_{z_x} respectively.

In the usual calculations the upper and ground state rovibrational wavefunctions are expanded as:

$$|v', J'K'_aK'_c\rangle = \sum_{v' \in B'} \sum_{K', \gamma'} C_{v', K'}^{\gamma' K'} |v'\rangle |J'K'\gamma'\rangle, \quad (18)$$

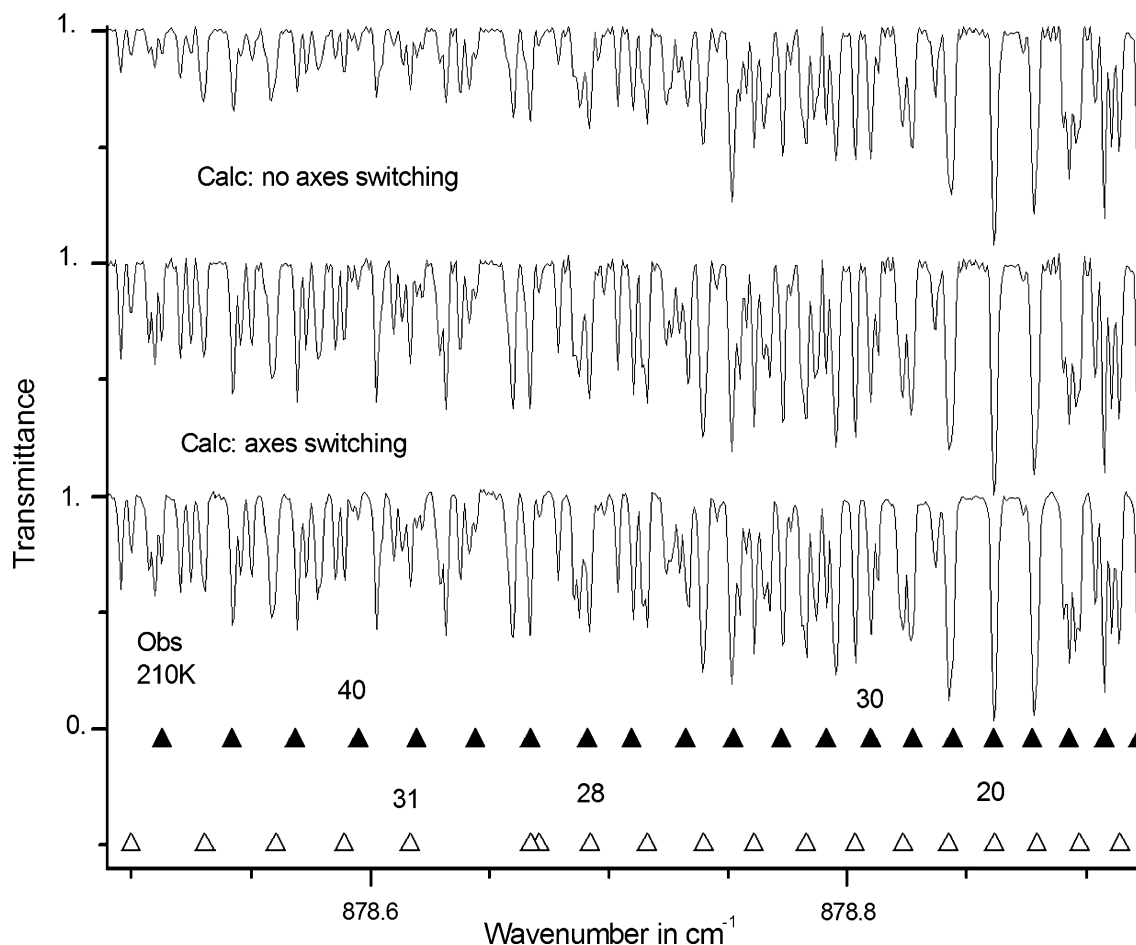


Fig. 6. Part of the spectrum in the 877.5–879.2 cm^{-1} region. The lower trace is the observed spectrum recorded at 210 K. As in Fig. 5 both the medium and upper traces were calculated using the same set of Hamiltonian and transitions moments constants (see Table 3 and Table 5, and [43]). It is clear that the axis switching effect has to be taken into account. In the upper trace the intensity pattern is indeed in strong disagreement with the observed spectrum. The quoted assignments are for $^Q Q$ -type transitions with $K'_a = J' - K'_c$ and $K'_c = 0$ (black triangles), $K'_c = 1$ (open triangles). A perturbation is clearly observable for $J = 29$ to $J = 30$ (see [16]) in the $K'_c = 1$ series.

$$|v = 0, JK_a K_c\rangle = \sum_{K''} C_0^{v''K''} |JK''\gamma''\rangle. \quad (19)$$

In Eqs. (18) and (19), the $C_0^{v''K''}$ coefficients are obtained from the diagonalization of the Hamiltonian matrices.

Now, as it was pointed out previously, we are facing the problem that the references axes (z, x, y) for the $\{5^1, 9^2\}$ excited states differ substantially from the inertial axes (a, b, c) which have been used to calculate the ground state energy levels. They are indeed tilted anticlockwise by the angles $\alpha_5 \sim 13.08^\circ$ and $\alpha_{99} \sim 8.97^\circ$ for the 5^1 and 9^2 vibrational states respectively as compared to the inertial axes (see Fig. 4).

To solve the problem one solution is to re-write the ground state wavefunctions using a new reference system of axes which is consistent with the 5^1 and 9^2 reference systems. This “new” reference system is obtained by an anticlockwise rotation of α_0 around the c axis using for α_0 the mean value of the 5^1 and 9^2 switching angles (see Eq. 10). The axes switching in the ground state is then performed using the Wigner tensorial ap-

proach and the $d_{K,K'}^{(J)}(\alpha_0)$, matrix elements. More explicitly for the $v = 0[J, K_a, K_c]$ energy levels with $J + K_c = \text{even}$ (resp. with $J + K_c = \text{odd}$), the “new” expansion of the ground state wavefunctions takes the form:

$$|v = 0, JK_a K_c\rangle = \sum_{\substack{K''\gamma'' \in \{E^+, O^-\} \\ \text{or } K''\gamma'' \in \{E^-, O^+\}}} \alpha_0 C_0^{v''K''} |^{\alpha_0} JK''\gamma''\rangle. \quad (20)$$

This new expansion is performed simultaneously on the E^+ and O^- Wang’s type bases (resp. on both E^- and O^+) whereas in Eq. (19) the summation on K'' is performed on one of the four Wang’s type reference bases E^+ or E^- or O^+ or O^- defined by:

$$\begin{aligned} |JK\gamma\rangle &= 1/\sqrt{2}(|J, K\rangle + \gamma|J, -K\rangle), \quad \text{for } K \neq 0, \\ |J0+\rangle &= |J, K\rangle, \quad \text{for } K = 0 \end{aligned} \quad (21)$$

with $\gamma = \pm 1$ and E^\pm for $K = \text{even}$ and O^\pm for $K = \text{odd}$.

The relationship between the “new” and “original” wavefunctions is given by:

$$\langle {}^{\alpha_0}JK'\gamma' | JK''\gamma'' \rangle = \left(d_{K',K''}^{(J)}(\alpha_0) + \gamma'(-1)^{K'-K''} d_{K',-K''}^{(J)}(\alpha_0) \right) \quad (22)$$

leading to:

$${}^{\alpha_0}C_0^{J'K'} = \sum_{K''} C_0^{J''K''} \left(d_{K',K''}^{(J)}(\alpha_0) + \gamma'(-1)^{K'-K''} d_{K',-K''}^{(J)}(\alpha_0) \right). \quad (23)$$

If either K' or K'' is equal to zero (but not both) the term on the right hand side of Eqs. (22) and (23) must be divided by $2^{1/2}$; if both K' and K'' are equal to zero, one has:

$$\langle {}^{\alpha_0}JK' = 0 \gamma' = +1 | JK'' = 0 \gamma'' = +1 \rangle = d_{0,0}^{(J)}(\alpha_0) \quad (24)$$

We have used this formalism to calculate the line intensities.

An alternative solution would have been to use for the computation of the ground state wavefunctions a rotational Hamiltonian which possesses artificially a non-orthorhombic term similar to the one used in the upper 5^1 and 9^2 excited states. In this case the Hamiltonian matrix would involve, in addition to the Watson's type operator, a $h_0\{J_x, J_z\}$ non-orthorhombic operator, with h_0 fixed at the average value $h_0 = 1/2(h_5 + h_{99})$ of the corresponding 5^1 and 9^2 parameters. We have checked that such a method gives identical results as the method described immediately above.

7.2. Line intensity calculation

The transition moment constants (see Eq. (17)) were determined through a least squares fit of the experimental intensities measured recently in [18] removing those lines which were identified as being strongly blended. This removal procedure could be done easily since our prediction is more complete than the one presently available on HITRAN. The experimental intensities are given at a temperature of 299 K and for a "natural" isotopic sample of nitric acid, so for the calculations we took into account both the $Z(299\text{ K})$ value and the $\text{H}^{14}\text{N}^{16}\text{O}_3$ isotopic abundance ($a = 0.989$).

The quality of the fit is very good as can be seen from the statistical analysis of the results given in Table 5. It is worth noticing that only three transition moment constants ${}^5\mu_z^1$, ${}^{99}\mu_z^1$ and ${}^{99}\mu_x^1$ (see Table 5) are necessary to reproduce the whole set of extensive line intensities. Also, since ${}^5\mu_z^1$ is about 10 times larger than both ${}^{99}\mu_z^1$ and ${}^{99}\mu_x^1$, the present model demonstrates clearly that the bulk of the intensity of the lines of the $2\nu_9$ band is borrowed from the ν_5 band. Finally the existence of the small ${}^{99}\mu_x^1$ term reflects the existence for $2\nu_9$ of a weak B -type component which exists together with the much stronger A -type component: such B -type transitions were clearly identified in the R branch (Fig. 2) allowing us to assign some unassigned lines quoted in Table 6 of [18].

Table 5

Transition moment constants for the ν_5 and $2\nu_9$ bands of HNO_3 and statistical analysis of the results of the line intensity calculation

	5^1	9^2
Transition moment constants (in Debye)		
ϕ_z	0.250132(320)	$-0.7375(230) \times 10^{-2}$
ϕ_x		$0.3068(200) \times 10^{-1}$
Statistical analysis of the results of the line intensity calculation ^a		
ν_5 and $2\nu_9$		
Number of transitions:	426	
$0 \leq \delta \leq 5\%$	53.8%	
$5\% < \delta \leq 10\%$	32.4%	
$10\% < \delta \leq 23\%$	13.8%	

The quoted errors are one standard deviation.

^a $\delta = |I_{\text{obs}} - I_{\text{calc}}|/I_{\text{obs}}$.

7.3. Synthetic spectrum

Using the vibrational energies, and the rotational, torsional and coupling constants given in Table 4 for the upper resonating $\{5^1, 9^2\}$ states and in [43] for the ground state, together with the transition moment constants given in Table 5 we have generated a comprehensive list of more than 100 000 line positions and intensities for the $\{\nu_5, 2\nu_9\}$ band system. The calculations were performed at 296 K for a "pure" isotopic sample of $\text{H}^{14}\text{N}^{16}\text{O}_3$ using an intensity cutoff of $0.1 \times 10^{-23} \text{ cm}^{-1}/(\text{molecule cm}^{-2})$, maximum values of 85 for J and 54 for K_a , maximum lower and upper energies of 2500 cm^{-1} and 3500 cm^{-1} , respectively. In this way, 112 418 lines were computed in the frequency range $806.2\text{--}964 \text{ cm}^{-1}$, and the total band intensities (i.e., the sum of the individual line intensities at 296 K) obtained are $S_{\text{Tot}}(\nu_5) = 1.027 \times 10^{-17} \text{ cm}^{-1}/(\text{molecule cm}^{-2})$ and $S_{\text{Tot}}(2\nu_9) = 0.750 \times 10^{-17} \text{ cm}^{-1}/(\text{molecule cm}^{-2})$.

When accounting for the contribution of the hot bands and of the other isotopic species these values correspond to an integrated band intensity for the region $810\text{--}960 \text{ cm}^{-1}$ of $2.31(12) \times 10^{-17} \text{ cm}^{-1}/(\text{molecule cm}^{-2})$.

It is interesting to compare our results with the previous ones:

Relative intensities. Figs. 1 and 2 show portions of a spectrum recorded at about 423 K around 845 and 925 cm^{-1} (P branch of ν_5 and R branch of $2\nu_9$) together with simulations performed using our results and the HITRAN linelist. It is clear that significant progress has been achieved.

Absolute intensities. The determination of the absolute intensities for HNO_3 lines is an overarching problem. A rather extensive comparison of the various measurements can be found in [18] showing the wide range of values obtained for the ν_5 and $2\nu_9$ band intensities. Since in this work we have fitted the

experimental intensities of [18] we found the same ratio (1.13) between our band intensities and the HITRAN ones. It is worth comparing our results with those recently obtained in [19] where an integrated intensity of $2.424(65) \times 10^{-17} \text{ cm}^{-1}/(\text{molecule cm}^{-2})$ was measured for the range 820–950 cm^{-1} . This value is only 5% larger than the value obtained in this work and the two values agree to within the experimental errors. In the absence of new measurements and, given the quality of both experimental teams, a suggestion would be to use for atmospheric applications the average value i.e., $2.367 \times 10^{-17} \text{ cm}^{-1}/(\text{molecule cm}^{-2})$.

8. Conclusion

Based on the data available in the literature, on new Fourier transform spectra recorded in Giessen and on new rotational transitions recorded in the centimeter spectral region in Kiel, a new calculation of the ν_5 and $2\nu_9$ bands of HNO_3 has been performed. The theoretical models which were used to calculate the line positions and intensities account for (i) the very strong resonances (Fermi and Coriolis) which perturb the 5^1 and 9^2 rotational levels, (ii) the axis switching effects, and (iii) the torsional splittings. In this way it proved possible to generate a significantly improved list of line positions and intensities for the ν_5 and $2\nu_9$ bands of HNO_3 . These results should lead to noticeably improved atmospheric HNO_3 retrievals.

Acknowledgments

The authors are deeply indebted to Dr. Jon T. Hougen for a careful reading of the manuscript and for numerous encouragements during this work. Dr. B.P. Winnewisser's comments on the manuscript are greatly appreciated. Moreover the authors thank gratefully Drs. L.R. Brown, R.A. Toth, E.A. Cohen, C. Chackerian, S.W. Sharpe, and Th.A. Blake for making available to them their results prior to publication and Dr. Laurent Coudert for valuable suggestions. Financial support from the French "Programme National de Chimie Atmosphérique" of the Centre National de la Recherche Scientifique" is gratefully acknowledged. The experimental work in Giessen and Kiel was supported in part by the Deutsche Forschungsgemeinschaft and the Fonds der Chemischen Industrie. Three of the authors (J.-M.F., J.O., and M.W.) thank the organizers of the workshop on Laboratory Spectroscopic Needs for Atmospheric Sensing, San Diego 22–26 October 2001 for their invitation. There this project was discussed. M.W. thanks NASA for its support.

References

- [1] World Meteorological Organization (WMO), Global Ozone Research and Monitoring Project, Rep. 44, Scientific Assessment of Ozone Depletion: 1998. Geneva, 1999.
- [2] J.M. Russell II, C.B. Farmer, C.P. Rinsland, R. Zander, L. Froidevaux, G.C. Toon, B. Gao, J. Shaw, M. Gunson, J. Geophys. Res. D 93 (1988) 1718–1736.
- [3] H. Oelhaf, T. Von Clarmann, H. Fischer, F. Friedl-Vallon, Ch. Frizsche, A. Linden, Ch. Piesch, M. Seefeldner, W. Völker, Geophys. Res. Lett. 21 (1994) 1263–1266.
- [4] C. Camy-Peyret, S. Payan, P. Jeseck, Y. Té, C. R. Acad. Sci. Paris Ser. IV 2 (2001) 905–922.
- [5] C.P. Rinsland, R. Zander, P. Demoulin, J. Geophys. Res. D 96 (1991) 9379–9389.
- [6] J.-M. Flaud, A. Perrin, J. Orphal, Q. Kou, P.M. Flaud, Z. Dutkiewicz, C. Piccolo, J. Quant. Spectrosc. Radiat. Trans. 77 (2003) 355–364.
- [7] A. Perrin, J.-M. Flaud, C. Camy-Peyret, B.P. Winnewisser, S. Klee, A. Goldman, F.J. Murcray, R.D. Blatherwick, F.S. Bonomo, D.G. Murcray, J. Mol. Spectrosc. 166 (1994) 224–243.
- [8] A. Perrin, J.-M. Flaud, C. Camy-Peyret, A. Goldman, C.P. Rinsland, M.R. Gunson, J. Quant. Spectrosc. Radiat. Trans. 52 (1994) 319–322.
- [9] A. Goldman, T.G. Kyle, F.S. Bonomo, Appl. Opt. 10 (1971) 65–73.
- [10] F.P. Giver, F.P.J. Valero, D. Goorvitch, F.S. Bonomo, J. Opt. Soc. Am. B 1 (1984) 715–722.
- [11] S.T. Massie, A. Goldman, D.G. Murcray, J.C. Gille, Appl. Opt. 24 (1985) 3426–3427.
- [12] P. Brockman, C.H. Bair, F. Allario, Appl. Opt. 17 (1978) 91–100.
- [13] A.G. Maki, J.S. Wells, J. Mol. Spectrosc. 108 (1984) 17–30.
- [14] T. Giesen, M. Harter, R. Schieder, G. Winnewisser, K.M.T. Yamada, Z. Naturforsch. A 43 (1988) 402–406.
- [15] A.G. Maki, J.S. Wells, J. Mol. Spectrosc. 152 (1992) 69–79.
- [16] A. Perrin, V. Jaouen, A. Valentin, J.-M. Flaud, C. Camy-Peyret, J. Mol. Spectrosc. 157 (1993) 112–121.
- [17] A. Perrin, J.-M. Flaud, C. Camy-Peyret, V. Jaouen, R. Farrenq, G. Guelachvili, Q. Kou, F. Le-Roy, M. Morillon-Chapey, J. Orphal, M. Badaoui, J.-Y. Mandin, V. Dana, J. Mol. Spectrosc. 160 (1993) 524–532.
- [18] R.A. Toth, L.R. Brown, E.A. Cohen, J. Mol. Spectrosc. 218 (2003) 151–168.
- [19] Ch. Chackerian, S.W. Sharpe, T.A. Blake, J. Quant. Spectrosc. Radiat. Trans. 82 (2003) 429–441.
- [20] T.M. Goyette, Ch.D. Paulse, L.C. Oesterling, F.C. De Lucia, P. Helminger, J. Mol. Spectrosc. 167 (1994) 365–374.
- [21] T.M. Goyette, L.C. Oesterling, D.T. Petkie, R.A. Booker, P. Helminger, F.C. De Lucia, J. Mol. Spectrosc. 175 (1996) 395–410.
- [22] D.T. Petkie, T.M. Goyette, P. Helminger, H.M. Pickett, F.C. De Lucia, J. Mol. Spectrosc. 208 (2001) 121–135.
- [23] L.S. Rothman, C.P. Rinsland, A. Goldman, S.T. Massie, D.P. Edwards, J.M. Flaud, A. Perrin, C. Camy-Peyret, V. Dana, J.-Y. Mandin, J. Schroeder, A. McCann, R.R. Gamache, R.B. Wattson, K. Yoshino, K.V. Chance, K.W. Jucks, L.R. Brown, V. Nemtchinov, P. Varanasi, J. Quant. Spectrosc. Radiat. Trans. 60 (1998) 665–710.
- [24] A. Goldman, C.P. Rinsland, A. Perrin, J.-M. Flaud, J. Quant. Spectrosc. Radiat. Trans. 60 (1998) 851–861.
- [25] N. Jacquinet-Husson, E. Arié, J. Ballard, A. Barbe, G. Bjoraker, B. Bonnet, L.R. Brown, C. Camy-Peyret, J.P. Champion, A. Chédin, A. Chursin, C. Clerbaux, G. Duxbury, J.M. Flaud, N. Fourrié, A. Fayt, G. Graner, R. Gamache, A. Goldman, V.I. Golovko, G. Guelachvili, J.M. Hartmann, J.C. Hilico, J. Hillman, G. Lefevre, E. Lellouch, S.N. Mikhailenko, O.V. Naumenko, V. Nemtchinov, D.A. Newnham, A. Nikitin, J. Orphal, A. Perrin, D.C. Reuter, C.P. Rinsland, L. Rosenmann, L.S. Rothman, N.A. Scott, J. Selby, L.N.

- Sinitsa, J.M. Sirota, M.A. Smith, K.M. Smith, V.I.G. Tyuterev, R.H. Tipping, S. Urban, P. Varanasi, M. Weber, *J. Quant. Spectrosc. Radiat. Trans.* 62 (1999) 205–254.
- [26] A. Goldman, C.P. Rinsland, *J. Quant. Spectrosc. Radiat. Trans.* 48 (1992) 653–666.
- [27] A. Goldman, C.P. Rinsland, F.J. Murcray, R.D. Blatherwick, D.G. Murcray, *J. Quant. Spectrosc. Radiat. Trans.* 52 (1994) 367–377.
- [28] A. Perrin, *Spectrochim. Acta A* 54 (1998) 375–392.
- [29] J.-M. Flaud, C. Piccolo, B. Carli, A. Perrin, L.H. Coudert, J.-L. Teffo, L.R. Brown, *J. Atmos. Ocean Opt.* 16 (2003) 172–182.
- [30] L.H. Coudert, A. Perrin, *J. Mol. Spectrosc.* 172 (1995) 352–368.
- [31] H.M. Pickett, *J. Mol. Spectrosc.* 148 (1991) 371–377.
- [32] H.M. Pickett, *J. Chem. Phys.* 107 (1997) 6732–6735.
- [33] L.R. Brown, C.B. Farmer, C.P. Rinsland, R. Zander, Remote sensing of the atmosphere by high resolution infrared absorption spectroscopy, in: K. Narahari Rao (Ed.), *Spectroscopy of the Earth's Atmosphere and Interstellar Medium*, Academic Press, Boston, 1992, pp. 97–151.
- [34] J.-M. Flaud, A. Perrin, High resolution infrared spectroscopy and one dimensional large amplitude motion in asymmetric tops: HNO_3 and H_2O_2 , in: D. Papoušek (Eds.), *Vibration-Rotational Spectroscopy and Molecular Dynamics*, Advanced Series in Physical Chemistry, World Scientific Publishing Company, Singapore, 1997, pp. 396–460 (Chapter 7).
- [35] R.L. Crownover, R.A. Booker, F.C. De Lucia, P. Helminger, *J. Quant. Spectrosc. Radiat. Trans.* 40 (1988) 39–46.
- [36] C.D. Paulse, L.H. Coudert, T.M. Goyette, R.L. Crownover, P. Helminger, F.C. De Lucia, *J. Mol. Spectrosc.* 177 (1996) 9–18.
- [37] K. Sarka, D. Papoušek, J. Demaison, H. Mäder, H. Harder, in: D. Papoušek (Ed.), *Advanced Series in Physical Chemistry*, vol. 9, World Scientific Publishing, Singapore, 1997.
- [38] V. Meyer, W. Jäger, R. Schwarz, H. Dreizler, *Z. Naturforsch. A: Phys. Sci.* 46 (1991) 445–449.
- [39] L. Albinus, J. Spieckermann, D.H. Sutter, *J. Mol. Spectrosc.* 133 (1989) 128–147.
- [40] S.P. Davis, J.W. Brault, M.C. Abrams, *Fourier Transform Spectrometry*, Academic Press, San Diego, 2001.
- [41] A.G. Maki, J.S. Wells, *J. Res. Nat. Inst. Stand. Techn.* 97 (1992) 409–470.
- [42] R. Schermaul, J.W.G. Seibert, G.Ch. Mellau, M. Winnewisser, *Appl. Opt.* 35 (1996) 2884–2890.
- [43] A. Goldman, J.B. Burkholder, C.J. Howard, R. Escribano, A.G. Maki, *J. Mol. Spectrosc.* 131 (1988) 195–200.
- [44] J.K.G. Watson, Aspects of quartic and sextic centrifugal effects on rotational energy levels, in: J. Durig (Ed.), *Vibrational Spectra and Structure*, Elsevier, 1977, Chap 1.
- [45] A. Perrin, J.-M. Flaud, M. Smirnov, M. Lock, *J. Mol. Spectrosc.* 203 (2000) 175–189.
- [46] A. Perrin, J.-M. Flaud, L. Margulès, J. Demaison, H. Mäder, S. Wörmke, *J. Mol. Spectrosc.* 216 (2002) 214–224.
- [47] J.T. Hougen, *J. Mol. Spectrosc.* 114 (1985) 395–426.
- [48] L.H. Coudert, J.T. Hougen, *J. Mol. Spectrosc.* 130 (1988) 86–119.
- [49] L.H. Coudert, J.T. Hougen, *J. Mol. Spectrosc.* 139 (1990) 259–277.
- [50] A.R. Edmonds, *Angular Momentum in Quantum Mechanics*, Princeton University Press, Princeton, NJ, 1960.
- [51] A.P. Cox, M.C. Ellis, C.J. Atfield, A.C. Ferris, *J. Mol. Struct.* 320 (1994) 91–106.
- [52] E.B. Wilson, J. Decius, P.C. Cross, *Molecular Vibrations*, McGraw-Hill, New York, 1955.
- [53] A. Perrin, in: *Proceeding of the XIV-th symposium on High Resolution Spectroscopy HighRuss*, July 2003, S.P.I.E 5311, 2003, pp. 25–32.
- [54] T.R. Huet, M. Godefroid, M. Herman, *J. Mol. Spectrosc.* 144 (1990) 32–43.
- [55] J.T. Hougen, J.K.G. Watson, *Canad. J. Phys.* 43 (1965) 298–320.
- [56] I. Ozkan, *J. Mol. Spectrosc.* 139 (1990) 147–162.
- [57] J.-M. Flaud, C. Camy-Peyret, R.A. Toth, *Water Vapour Line Parameters from Microwave to Medium Infrared*, Pergamon press, Oxford, 1981.
- [58] C. Camy-Peyret, J.-M. Flaud, Vibration-rotation dipole moment operator for asymmetric rotors, in: K. Narahari Rao (Ed.), *Molecular Spectroscopy Modern Research*, vol. 3, Academic Press, New York, 1985, pp. 69–110.